Hydrogel Composition Effects on Performance as Single-walled Carbon Nanotube Purification Media

Marshal Dolan†; Laurique N Hughes†; and Kevin Tvrdy†*

†Department of Chemistry & Biochemistry, University of Colorado at Colorado Springs, Colorado Springs, Colorado 80918, United States

*ktvrdy@uccs.edu

Abstract

Hydrogel microsphere media allows for post-synthetic purification of single-walled carbon nanotubes (SWNTs), affording characterization and application of their unique *(n,m)* chirality-dependent properties. This work reports the characterization of five hydrogel resins, Sephacryl S-100, S-200, S-300, S-400, and S-500, and the implementation of each as a SWNT purification medium. The physiochemical properties of each resin were explored spectroscopically, through elemental analyses, and with both light and electron microscopy. Both surface porosity and hydrogel swelling ratio were found to increase as the concentration of component allyl dextran (aDEX) decreased, each with increasing Sephacryl S-number. Conversely, invariant properties included hydrogel microsphere size distribution and concentrations of components methylene bis acrylamide and ammonium persulfate. When employed within gel-based SWNT purification schemes in overloading conditions, Sephacryl formulations of larger S-number adsorbed fewer SWNTs, but the chirality dependence of SWNT adsorption and elution efficiency were approximately consistent across all resins. In underloading conditions, approximately one third of introduced SWNTs passed through each resin unabsorbed, while the resins showed varying chirality-dependent adsorption efficiencies. These observations collectively identify aDEX-rich gel regions as responsible for SWNT purification, along with a SWNT-exclusive parameter other than chirality (speculated as length) that convolutes the effectiveness of gel-based single-chirality purification.

Introduction

Single-walled carbon nanotubes (SWNTs) are one-dimensional analogues of graphene that, depending on the per-tube geometric chiral wrapping vector *(n,m)*, can exhibit metallic or semiconducting properties.[1] Approximately two-thirds of bulk-synthesized SWNTs are semiconducting, with bandgaps that correspond with the *(n,m)*, or chirality, of each tube.[2] Further, semiconducting SWNTs exhibit relatively large absorbance cross sections[3] with narrow absorbance and emission bandwidths in the near infrared region of the spectrum.[4] Collectively, the diverse properties of SWNTs, coupled with their exclusive composition of earth abundant carbon, make them ideal materials for a wide range of electronic, sensing, imaging, thin film, and structural devices.[5–10] However, because current methods of bulk-scale SWNT production necessarily generate many SWNT chiralities simultaneously, post-synthetic purification is needed to isolate *(n,m)* chiralities with electronic or structural properties to match the needs of a given application. Among the various strategies developed to achieve such purification,[11–25] iterative hydrogel-based interactions[26,27] have emerged as an effective, scalable, and cost effective approach.[28] The work presented herein focuses on both quantifying and understanding the purification ability of the commercially available Sephacryl series of gels, with a specific focus on correlating per-gel chemical and physical properties with SWNT chiral selectivity and overall process efficiency. Results reported herein advance the understanding of chirality specific SWNT interactions with hydrogels, information which will collectively be used in the rational design of novel, SWNT-specific hydrogel purification media.

Beds of hydrogel microspheres were first used by Kappes and coworkers to purify SWNTs based on electronic type, using gradients of sodium dodecyl sulfate (SDS) surfactant, to control adsorption and subsequent elution of SWNTs to agarose-based gels.[26] Kataura and coworkers then modified this approach by combining Sephacryl S-200 with concentrated SWNT suspensions to create overloading conditions capable of isolating a handful of SWNTs *(n,m)* with exceptionally high single-chirality purity.[27] Both modeling[29,30] and experimental modulations of this approach involving perturbation of the

temperature,[31] surfactant,[32] Sephacryl S-200 microsphere diameter,[33] and ultrasonication processing procedure[34] have afforded advancements in both understanding and realization of single-chirality SWNT purification. However, the role of the hydrogel media remains relatively unexplored, with each of the aforementioned studies exclusively using Sephacryl S-200, a porous material manufactured for the chromatographic purification of proteins with a size exclusion limit of 250 kDa for globular proteins. Conversely, our group has recently demonstrated that SWNT interactions with Sephacryl S-200 are relegated to the surface of the gel microspheres,[33] suggesting that the chirality-specific interactions between SWNTs and gel that afford SWNT purification are driven by the physiochemical surface properties of the gel as opposed to its interior porosity. This phenomenon has been further demonstrated by reports from our group[35] and others[36–39] that show unique, less chirally selective, interactions between SWNTs and hydrogels other than Sephacryl S-200. Here, we focus on the unique chemical and physical properties among the five commercially available types of Sephacryl, namely S-100, S-200, S-300, S-400, and S-500, and how each performs as SWNT purification media.

Dextran-based hydrogels (such as Sephacryl) were developed in the late 1950s and 1960s by Per Magnus Flodin and coworkers at Pharmacia AB (Uppsala, Sweden)[40] as novel materials capable of chromatographic isolation of biomolecules[41] based on variations of its interior porosity. Presently, Sephacryl is sold commercially by Cytiva® and is available in five different formulations, each exhibiting a different biomolecule fractionation range (pore size). Each Sephacryl formulation is sold as a slurry of hydrogel microspheres with a reported average diameter of approximately 25 - 75 μm, which can be packed within a column, as commonly utilized within Fast Protein Liquid Chromatography (FPLC) schemes. Previously, our group used an atomistic model informed by experimental elemental analysis to approximate the chemical formulation of Sephacryl S-200, which is comprised of allyl dextran (aDEX) crosslinked with methylene bis acrylamide (MBA), collectively formed through free-radical polymerization using ammonium persulfate (APS) free radical initiator.[42] Given the remarkable effectiveness of Sephacryl

S-200 at generating chirally-pure aliquots of several small diameter chiralities, and because all Sephacryl resins are reported to be crosslinked copolymers of aDEX and MBA, it is worthwhile to assess the physical and chemical properties of each Sephacryl resin and correlate such with their performance as a SWNT purification medium.

This work presents the characterization of each of five Sephacryl resins by interpretation of elemental analysis within an atomistic framework of the Sephacryl formulation, Fourier transform infrared spectroscopy (FTIR) analysis, assessment of hydrogel swelling ratio, and direct imaging of both the gel microsphere size distribution by light microscopy and the nanoscale surface morphology by electron microscopy. These per-gel properties are compared with the ability of each resin to adsorb and elute SWNTs in a chirally selective manner, which was performed experimentally under both overloading (# SWNTs >> # gel binding sites) and underloading (# gel binding sites >> SWNTs) conditions. Importantly, strong correlations between Sephacryl surface morphology and total SWNT uptake, as well as between Sephacryl aDEX content and SWNT chiral selectivity are noted, and a case for using Sephacryl S-100, and not S-200, as the standard SWNT purification media is presented. Collectively, this work stands to benefit both researchers seeking to effectively purify SWNTs for implementation within novel devices and schemes, as well as those seeking to understand and advance gel-based SWNT purification methods.

Materials and Methods

Materials. Sephacryl S-100 (High Resolution, Lot: 10288932), Sephacryl S-200 (High Resolution, Lot: 10240334), Sephacryl S-300 (High Resolution, Lot: 10290265), Sephacryl S-400 (High Resolution, Lot: 10289140), and Sephacryl S-500 (High Resolution) were purchased from Fisher Scientific and used as received, homogenizing each using repeated gentle inversion. Single-walled Carbon Nanotubes, synthesized using the CVD-based CoMoCAT method were obtained from Sigma Aldrich (Signis SG65i, 773735-1G, Lot: MKCP4753) and reported to contain approximately ≥95% semiconducting species

enriched 41% in the *(6,5)* chirality. Sodium dodecyl sulfate (≥99.0%, 74255-250G, Lot: STBK5566), sodium borohydride (98%, 45,288-2, Lot:CO10711MI), and N,N'-methylene bisacrylamide (MBA, 99%, 146072-100G, MKCL1331) were each purchased from Sigma Aldrich and used as received. Dextran (Alfa Aesar, J63789, Lot: M10G032), allyl-bromide (Alfa Aesar, 99%, A11766, Lot: 10194833), sodium hydroxide (S318-500, Lot: 142402), and ammonium persulfate (BP179-100, Lot: 197012), were each purchased from Fisher Scientific and used as received. Aqueous suspensions employed deionized water (15MΩ resistivity).

Analysis of Sephacryl Resins. The spectroscopic (Fourier transform infrared spectroscopy, iD7 attenuated total reflectance attachment, spectral resolution < 1.0 cm^{-1} with Ordinate linearity < 0.15% deviation), surface (Scanning electron microscopy (SEM), Tescan VEGA3 SEM, VegaTC software), and compositional (Carbon, Hydrogen, Nitrogen, and Sulfur elemental analysis; Atlantic Microlabs; Norcross, GA; uncertainty of ±0.3%) characteristics of hydrogels were determined following flash freezing of a small volume (~ 1 mL) of hydrated gel using liquid nitrogen and subsequent lyophilization using a Savant SC110 SpeedVac chamber affixed to a Savant RVT4104 vapor trap held at -110°C. For SEM analysis, hydrogels were sputtered with an approximate gold thickness of 8.5 nm using a Standard Denton Desk V deposition system affixed with a gold target and integrated JB Industries DV-85N-250 Platinum Series Vacuum pump. For spectroscopic comparison between each Sephacryl resin and its synthetic components, allyl dextran was synthesized,[43] purified, and characterized by ^{1}H NMR (400 MHz, Bruker Biospin Corp.) to determine a substitution of σ=0.26 pendant allyl groups per dextran ring.[42]

To afford direct comparison between SWNT uptake and the elution properties of hydrogels with different compositions, each gel was characterized in terms of its microsphere surface per volume of homogenized gel suspension using:

$$A_N = \sum_i f_{sln.} f_{s.g.} \frac{6}{d_i} P(d_i) \Delta d_i \quad (1)$$

where A_N is the normalized surface area of a homogenized suspension of hydrogel microparticles in units of $cm^2\ mL^{-1}$, f_{sln} is the fractional contribution of the hydrogel volume in a homogenized suspension of particles, $f_{s.g.}$ is the fraction of particulate gel volume amongst a bed of packed hydrogel, and $P(d_i)$ is the probability of observing a particle of diameter d_i withing bin size Δd_i. Homogenized suspensions of hydrogel microspheres were allowed to settle under gravitational force to determine f_{sln}, while $f_{s.g.}$ is assumed to be 0.64 given irregular packing of spherical particles.[44] The distribution of gel microsphere diameter for a given resin, $P(d_i)$, was determined at 1 μm increments using optical microscopy (Leica DM750 M Binocular Materials Microscope, Leica ICC50 HD Camera, Leica Application Suite LAS EZ) and an image-based circular shape recognition script written in Mathematica. Additional details on hydrogel bed normalization by particle surface area is provided in our previous works.[33,42]

Preparation of Single-walled Carbon Nanotube Suspension. SWNT suspensions at 1 mg/mL in 70 mM SDS were created by transferring 20 mg of raw SWNT powder into a vial containing 10 mL of 70 mM SDS. The vial was bath sonicated (Fisher Scientific FS5) for 10 minutes to break apart large pieces of SWNT soot and transferred to a 50 mL jacketed beaker (Chemglass CG-1103-01). Two additional 5 mL aliquots of 70 mM SDS were then used to wash the vial and transfer residual SWNT into the jacketed beaker. The liquid was subjected to tip-horn sonication (Branson Digital Sonifier 250, 20kHz, ½" tip) at 20W (approximately 30% amplitude) for 4.0 hours while circulating chilled water (13°C, LM6 Benchtop Chiller) through the jacketed portion of the beaker. Immediately after sonication was completed, the suspension was ultracentrifuged at 185,701 average ×g (50k rpm, Sorvall MX 120 Plus Micro-Ultracentrifuge, S50-ST rotor) for 2.0 hours at 25°C, after which the top ~90% of liquid from each centrifuge tube was retained and assumed to contain individualized SWNTs in 70mM SDS. Following ultracentrifugation, the SWNT suspension was subjected to hydrogel pretreatment (a process described elsewhere[42]) to remove amorphous carbon and afford quantitation of SWNT uptake and elution with a single column scheme.

Column-based Purification of Single-walled Carbon Nanotubes. Each experiment was carried out in triplicate, with either direct or propagated error reported as the standard deviation of parallel measurments. Each hydrogel resin of known and normalized surface area was loaded into its own fritted column (Thermo Scientific 29920), alongside a control column absent of gel. All columns were equilibrated with three passes of 70 mM SDS of volume approximately 10 times that of the settled gel to remove storage solution and prepare the gel for interaction with SWNTs. A pretreated SWNT suspension was diluted with 70 mM SDS to achieve a maximum optical density in the E_{11} region of ~3.0 (Agilent 8453 absorbance spectrometer; 1 cm path length Sub-micro Quartz Spectrometer Cell, Starna Cells), 1.5 mL of which was introduced to the top of each column, allowed to pass via gravitational force, and collected. In the case of overloading conditions, the collected SWNTs were passed through the gel bed twice more to ensure equilibration of the SWNT suspension with the gel, while only a single pass was used in underloading conditions. After the final passage through each column, both the hydrogel beds (and gel-free control) were washed with 1.5 mL of neat 70 mM SDS which is collected in the same vial as the passed SWNTs. This washing step both ensured that any residual non-adsorbed SWNTs present in the interstitial space of the gel microspheres were removed, and that resulting SWNT suspensions were diluted to a maximum optical density ≤1.5, affording accurate characterization by absorbance spectroscopy. Differential analysis of the absorbance spectrum of the SWNT passing through the control column versus that passing through a gel-containing column afforded calculation of the absorbance characteristics of materials adsorbed to the gel. A fraction of adsorbed SWNTs were eluted from each gel-containing column through addition of 1.0 mL of 175 mM SDS, its passage via gravitational force, and its collection for spectroscopic analysis.

Quantitative Analysis of Absorbance Spectra. The absorbance spectrum of a typical SWNT suspension is comprised of peaks as associated phonon sidebands associated with electronic transitions from each chirality present, along with a featureless background from amorphous carbon. Absorbance spectra of

SWNT suspensions were analyzed with an in-house written Mathematica program. Briefly, this program seeks a least squares best-fit between a measured absorbance spectrum and sum of individual chiral contributions combined with a linear amorphous carbon background. An in-depth approach to this algorithm is detailed by Watts et al.[45] Because the SWNTs used were reported to contain ≥95% semiconducting species, only semiconducting species—specifically, the *(6,4)*, *(6,5)*, *(7,3)*, *(7,5)*, *(8,3)*, *(9,1)*, and *(10,2)* species—are fitted in the E_{11} region (850 nm – 1100 nm). Each E_{11} transition and an associated phonon sideband were fit with Lorentzian line shapes. The absorbance characteristics of each of the chiralities present in appreciable amounts within the SWNT material used in this study is fully characterized at wavelengths ≤ 1100 nm,[45] affording relatively straightforward characterization with silicon-based detectors.

Results and Discussion

As-purchased Sephacryl resins S-100, S-200, S-300, S-400, and S-500 were characterized in terms of both their chemical composition and physical properties. These materials represent each type of Sephacryl presently available for purchase. As the focus of this work is the interaction of each of these gels with SWNTs of varying *(n,m)* chirality, characterization was carried out in terms of the potential of each resin to interact with SWNTs within gel-based purification schemes. Specifically, SWNTs of varying *(n,m)* chirality are purified from a suspension of individualized (unbundled) tubes, each surrounded by a quasi-micelle of SDS molecules. Gel-based purification relies on surfactant concentration- or surfactant type-dependent interactions between SWNT and the hydrogel surface. The mechanism behind the dynamic interaction between SWNTs, surface-bound surfactant, and the hydrogel surface that affords SWNT purification is of great interest, and the role of the gel in this process is at the center of this work.

The chiral dependence of SWNT/gel interaction that affords gel-based purification may be due to the SWNT itself (SWNTs are electron accepting[46,47] and exhibit chirality dependent band structure[2]), the

properties of the surfactant associated with each tube (the SDS headgroup imparts a negative electrostatic charge to SWNT,[48] with the charge density of each tube—the number of SDS molecules per SWNT length—likely chirally dependent[49]), or some combination thereof. In contrast, the hydrogel media used to purify SWNTs—the focus of this work—can be thought of as having chemical properties that include the nature, density, and charge of its functional groups, in addition to physical properties that include the shape and porosity of its surface and interior. The following two subsections describe the chemical and physical characterization of each of five Sephacryl resins in terms of the properties expected to most significantly impact SWNT interaction. Following characterization of each gel, the next subsection describes how each resin performs as SWNT purification media, and the final subsection interprets such performance in terms of the characterizations made in the earlier parts of this work and an overarching mechanism of SWNT/gel interactions.

Characterization of Chemical Properties of Sephacryl Series Hydrogel Media. In chemical terms, the primary component of Sephacryl microspheres is, as is with hydrogels generally, water. Non-aqueous components of Sephacryl have been described as "the copolymer obtained by cross-linking allyl dextran with N,N'-methylene bis acrylamide by radical polymerization directly on to the allyl groups."[50] A recent study conducted by our group used elemental analysis and an atomistic model of the Sephacryl S-200 formulation to estimate the relative abundance of its non-aqueous components: allyl dextran (aDEX), methylene bis acrylamide (MBA), and radical initiator ammonium persulfate (APS), respectively.[42] The aDEX, MBA, and APS content of each of the five Sephacryl gels were assessed here using both Fourier transform infrared (FTIR) absorbance spectroscopy and elemental analysis.

First, all five Sephacryl gels were subjected to lyophilization and characterized using FTIR. Obtained spectra, along with those of aDEX, MBA, and APS (for comparison) are shown in **Fig. 1A** (following page). The spectral features of MBA include C=O stretching at 1657 cm^{-1}, C=C stretching at 1624 cm^{-1}, and N-H scissoring at 1521 cm^{-1}.[51–54] The spectral feature of APS includes S=O stretching at 1440 cm^{-1}, while

features of aDEX include bending of the C-O-C bond and glycosidic bridge at 1153 cm^{-1}, the C-O bond at the C_4 glucose position at 1106 cm^{-1}, chain flexing of the α(1,6) linkage 1012 cm^{-1}, and the α-glycosidic bond at 915 cm^{-1}.[55–57] A qualitative comparison of the intensity of these spectral features suggest that the concentrations of components MBA and APS are approximately unchanged across the five resins, while the concentration of aDEX generally decreases with increasing Sephacryl S-number.

A more quantitative assessment of the per-gel aDEX, MBA, and APS content was made through elemental analysis data terms of an atomistic model of an APS-initiated MBA-crosslinked water-free network of aDEX polymer. Experimentally, each as-received Sephacryl resin was washed thoroughly with water, lyophilized, and analyzed by C, H, N, S elemental analysis (Atlantic Mircolab; Norcross, GA), the results of which are specified in **Table 1** (following page). Two reasonable assumptions make it possible to translate data from **Table 1** into meaningful information about the chemical composition of each Sephacryl resin. First, it is assumed that each gel is a crosslinked combination of aDEX and MBA initiated by APS, which affords the relative abundance of carbon, hydrogen, nitrogen, and sulfur to be directly mapped onto the relative concentrations of aDEX (containing carbon, hydrogen), MBA (containing carbon,

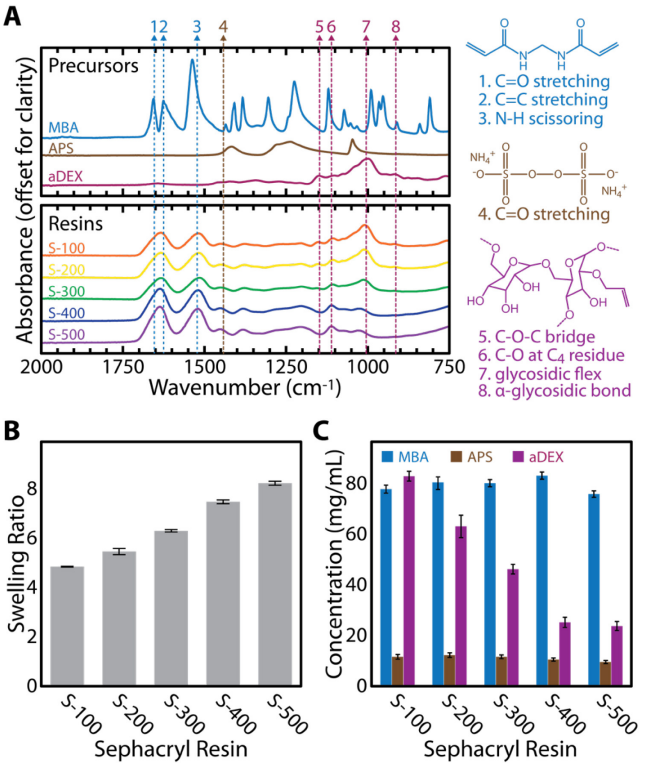

Fig. 1. Determination of the relative abundance of components aDEX, MBA, and APS within Sephacryl S-100, S-200, S-300, S-400, and S-500. (**A**) Comparison of the vibrational spectrum of the lyophilized product of each resin with that of each component, with component/resin areas of spectral overlap and corresponding structural assignments notated. (**B**) The swelling ratio of each resin .(**C**) A quantitative combination of per-resin swelling ratio, per-resin elemental analysis (**Table 1**), and an atomistic model of Sephacryl affords quantitative estimation of the concentration of each of aDEX, MBA, and APS components within the aqueous environment of each resin. The full height of error bars in (**B**) represent one standard deviation of triplicate measurement while those in (**C**) represent the propagated uncertainty associated with measurement of both swelling ratio and elemental analysis.

hydrogen, and nitrogen), and APS (containing nitrogen, hydrogen, and sulfur). Second, it is assumed that during synthesis the total aqueous volume of reactants translates directly to that of hydrogel formed, an observation that held true during our previous study of Sephacryl-like gels in block copolymer format.[42] This second assumption corresponds with the experimentally determined swelling ratio of each gel:

$$Swelling\ Ratio = \frac{mass_{hydrated} - mass_{dried}}{mass_{dried}}, \quad (2)$$

where $mass_{hydrated}$ and $mass_{dried}$ are the mass of the hydrogel microspheres (with interstitial liquid removed) before and after lyophilization, respectively, as shown for each resin in **Fig. 1B**. In terms of each of the five Sephacryl resins studied here, per-resin elemental analysis and per-resin swelling ratio are interpreted within the framework of the atomistic model to estimate the concentration of each Sephacryl component (APS, MBA, and aDEX) used to synthesize each resin. The results of this analysis are shown in **Fig. 1C**, while further details about these assumptions and the calculations they enable are described in **Supporting Information Section S1**.

Importantly, the qualitative interpretation of the FTIR spectra shown in **Fig. 1A** agrees with the results of the atomistic modeling shown in **Fig. 1C** and **Table 1**, which collectively suggest that the non-aqueous concentration of radical initiator APS and crosslinker MBA are approximately constant across all Sephacryl resins, while that of polysaccharide backbone aDEX decreases with increasing Sephacryl S-number. This

	Experimentally Determined Elemental Abundance in Dried Gel (wt%)				**Calculated Component Concentration in Hydrated Gel (mg/mL)**		
Resin	*C*	*H*	*N*	*S*	*APS*	*MBA*	*aDEX*
S-100	44.2	7.2	9.0	1.9	11.5 ± 1.8	77.2 ± 3.1	82.3 ± 3.8
S-200	45.6	7.0	10.4	2.2	12.2 ± 1.7	79.9 ± 4.9	62.7 ± 8.8
S-300	45.6	7.1	11.6	2.4	11.5 ± 1.5	79.6 ± 2.8	45.9 ± 3.8
S-400	46.7	7.1	13.8	2.5	10.4 ± 1.3	82.5 ± 2.9	25.0 ± 4.0
S-500	46.0	7.3	13.7	2.5	9.4 ± 1.2	75.3 ± 2.5	23.6 ± 3.5

Table 1. Quantitative results of elemental analysis (carbon, hydrogen, nitrogen, sulfur) of lyophilized hydrogels Sephacryl S-100, S-200, S-300, S-400, and S-500. These data, when combined with a presumption of knowledge of the components of Sephacryl copolymers from a previous study,[42] afford estimation of the per-component concentration of each Sephacryl resin, listed here and shown graphically in **Fig. 1C**. Error associated with elemental abundance is ±0.3wt%, while that of per-component concentration represent the propagated uncertainty associated with measurement of both swelling ratio and elemental analysis.

analysis provides chemical insight into the relative nature and density of chemical functional groups present among the five Sephacryl resins. This information both provides insight into the functionality of each Sephacryl resin as media for size-selective purification of biological macromolecules, and in terms of this study, the ability of each to adsorb and elute SWNTs in a chirally selective manner.

Characterization of Physical Properties of Sephacryl Series Hydrogel Media. In physical terms, Sephacryl presents as hydrogel microspheres approximately 37 ± 5 μm in diameter. The specific diameter distribution of each of the five resins studied here was measured by light microscopy, a representative image of which is shown for Sephacryl S-100, S-300, and S-500 in **Fig. 2A**, with associated size distributions for all five resins shown in **Fig. 2B**. Importantly, these distributions are necessary to normalize SWNT/gel interactions to the total surface area within a given gel bed, as the number of SWNTs adsorbed to Sephacryl S-200 has been shown to scale linearly with total microsphere surface area.[33]

On a smaller physical scale, Sephacryl contains nanoscale pores that afford its characteristic fractionation range when employed within FPLC schemes. Related to the physical size of each pore, the manufacturer provides a fractionation range for the use of Sephacryl to isolate both dextran (S-200 through S-500) and globular proteins (S-100 through S-400), each of which is summarized in **Supporting Information Table S.1**. The maximum value of each fractionation range was converted to a respective pore size, treating polymeric dextran chains as coiled spheres with associated hydrodynamic radii and proteins as globules. Additional details about these calculations are provided in **Supporting Information Section S2**. Owing to the extreme aspect ratio of SWNTs (length >> diameter), the pore size of each hydrogel (and not fractionation range) becomes the relevant parameter for modeling SWNT/gel interaction. The calculated pore size of each Sephacryl formulation in terms of both dextran and globular protein fractionation is shown in **Fig. 2C**, which demonstrates that Sephacryl resins designated with a larger S-number have larger pore sizes. This trend is further demonstrated by the experimentally measured swelling ratio of each Sephacryl formulation (**Fig. 1B**), which has been shown to correlate

proportionally with pore size.[58] Specifically, the non-water content of the resin with the smallest pores, S-100, was measured at 17.1% and that with the largest pores, S-500, measured at 10.8%.

Visual confirmation of this trend in pore size was achieved by imaging lyophilized (to remove water while preserving the structure of the non-aqueous components) beads of each Sephacryl formulation using scanning electron microscopy (SEM), **Fig. 2D**. These images demonstrate that the surface of Sephacryl S-500 has both more voids and larger voids than that of Sephacryl S-100, with an evident trend in both the number and relative size of voids increasing from S-100 to S-500. Given these images, the topology of each gel can generally be described as popcorn-like, with globular structures on the order 10s of nanometers which are bound together by a more smooth, continuous support matrix. The results of

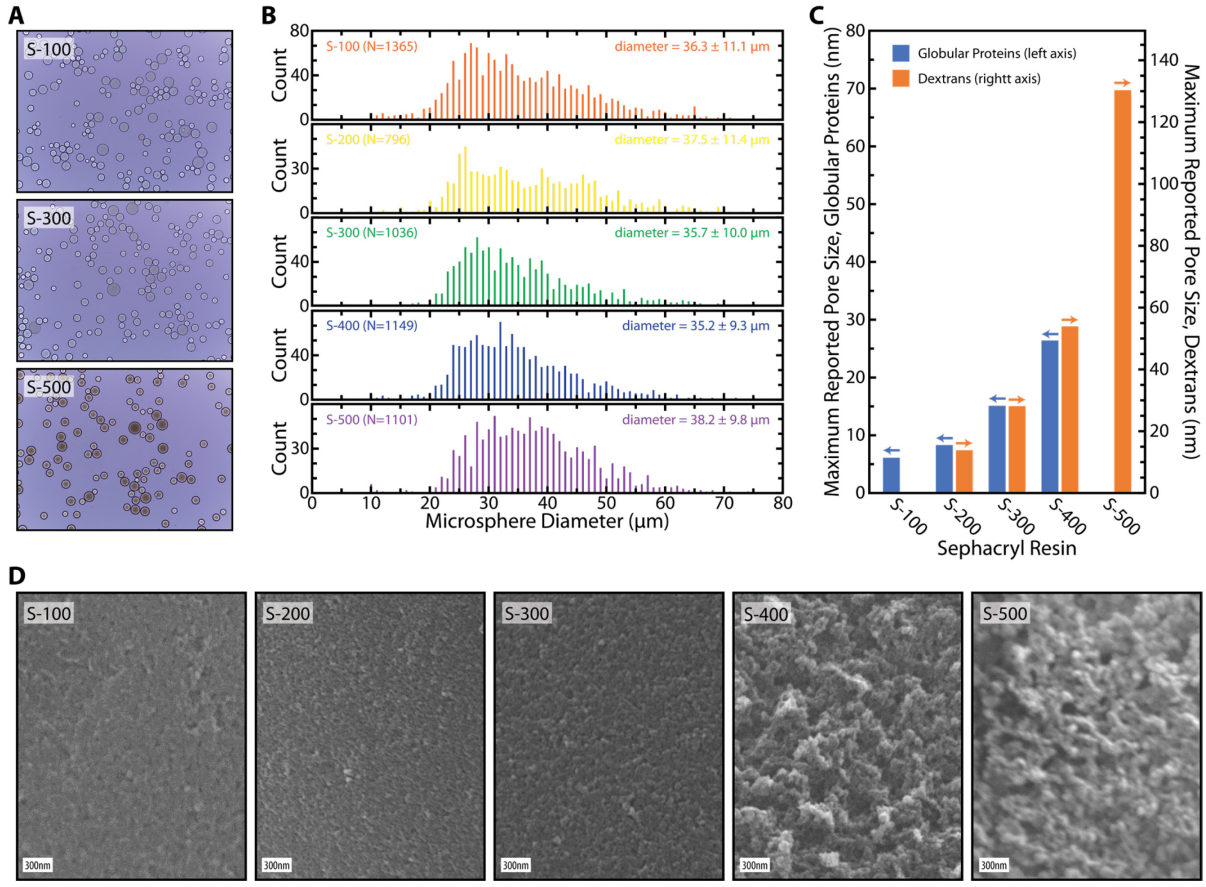

Fig. 2. Physical properties of Sephacryl resins. (**A**) Light microscopy and (**B**) corresponding size distributions of various Sephacryl resins. (**C**) Manufacturer provided maximum pore diameter for the size-selective purification of biological globular proteins and dextrans. Scanning electron microscopy, (**D**), of each of the five Sephacryl resins studied in this work.

this afford the assignment of the globular quasi-spherical structure to aDEX and that of the continuous support matrix to MBA. Previous studies of the morphology of dextran within aqueous solutions have found that it takes on a coil-like globular structure,[59] in agreement with this assignment.

In summary, the chemical and physical properties of each commercially available Sephacryl formulation have been characterized in terms of their expected effect on SWNT/gel interaction. While the physical diameter of each hydrogel bead is constant across each resin, as are the non-aqueous component concentrations of radical initiator APS and crosslinker MBA, the concentration of polysaccharide backbone aDEX decreases with increasing Sephacryl S-number. The relative decrease in concentration of aDEX results in an increase of both swelling ratio and pore diameter with increasing Sephacryl S-number. In terms of anticipated SWNT interaction, the pore size of each Sephacryl formulation is far less than the length of SWNTs purified using hydrogel-based methods, suggesting that SWNTs do not enter the porous interior of Sephacryl beads, and instead SWNT/Sephacryl interactions are relegated exclusively to the surface of the gel, in agreement with previous studies.[33] The topological surface of Sephacryl formulations with larger S-number is more rough on the expected scale of SWNT length (≈300 nm), and appears to be dominated by protruding quasi-spherical structures with an underlying support matrix. This characterization is summarized in **Fig. 3**, in which pore size, MBA content, and aDEX content is depicted spatially for Sephacryl S-100, S-300, and S-500, with corresponding color identifiers. The ability of each gel is to adsorb and elute SWNTs in a chirality dependent manner is quantified and described in the following section, which is followed by an overarching analysis of correlations between per-gel characterization and SWNT/gel interactions.

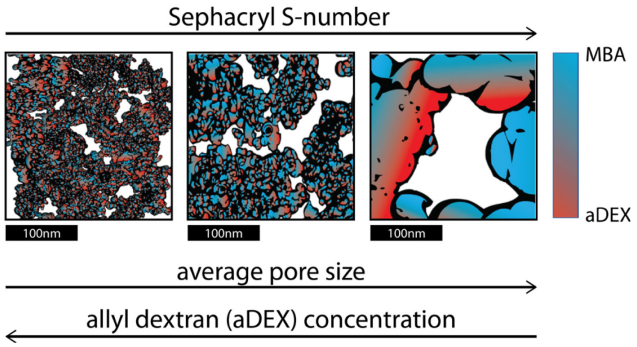

Fig. 3. Model illustration highlighting the chemical and physical properties of Sephacryl resins studied in this work.

Characterization of SWNT Purification Properties of Sephacryl Series Hydrogel Media. In general terms, hydrogel-based SWNT purification schemes involve the iterative passage of aqueous suspensions of SWNTs with relatively low (70mM) SDS concentration through beds of hydrogel microspheres. For a given gel bed, the relative ratio of SWNTs passed (# SWNTs) to that of gel adsorption sites present (# gel sites) is selected to produce either overloading (# SWNTs >> # gel sites) conditions in which SWNT chiral *(n,m)* selectivity is maximized,[31] or underloading (# SWNTs << # gel sites) conditions in which mechanistic aspects of the SWNT/gel interaction can be investigated.[45] Following washing of gel beds with neat aqueous 70 mM SDS to rid the interstitial gel space of non-adsorbed SWNTs, a fraction of SWNTs adsorbed to the gel is eluted through passage of relatively high (175 mM) SDS, which is collected as an eluent purified by SWNT chirally *(n,m)*. Illustrations of the experimental setup and eluants collected in a single-column gel-based SWNT purification scheme are available elsewhere.[45] Here, we report the quantitative results of critical purification parameters related to the efficiency of SWNT adsorption to each Sephacryl series gel, SWNT elution from each, and the chiral *(n,m)* selectivity of both processes. Importantly, the microsphere size distribution of each resin (see **Fig. 2B**) was used to ensure that each resin tested contained equivalent total microsphere surface area.

The use of overloading conditions ensures that the SWNT *(n,m)* chiralities that are most kinetically and thermodynamically favorable to adsorb to the gel surface do so preferentially, allowing less favorable chiralities to pass through the bed unadsorbed. Following washing, the elution of a portion of adsorbed materials produces chirally purified suspensions of SWNTs that can be used for downstream applications. Here, overloading conditions were employed with approximately a 6:1 ratio of introduced SWNTs per gel

binding site, with total gel binding sites (per cm^2 gel surface area) having been determined from previous studies of Sephacryl S-200.[33] The absorbance spectra of a SWNT suspension divided and passed through gel beds of each of Sephacryl S-100, S-200, S-300, S-400, and S-500, each presenting 229 cm^2 of microsphere surface area, are shown in **Fig. 4A**. Also shown is the absorbance spectrum of the SWNT suspension passed through a gel-free control column. Comparatively, SWNT suspensions following passage through Sephacryl of any formulation contain fewer SWNTs than that following passage through the gel-free control, as indicated by their relatively smaller absorbance in the characteristic E_{11} region (800 - 1100 nm) of the spectrum.

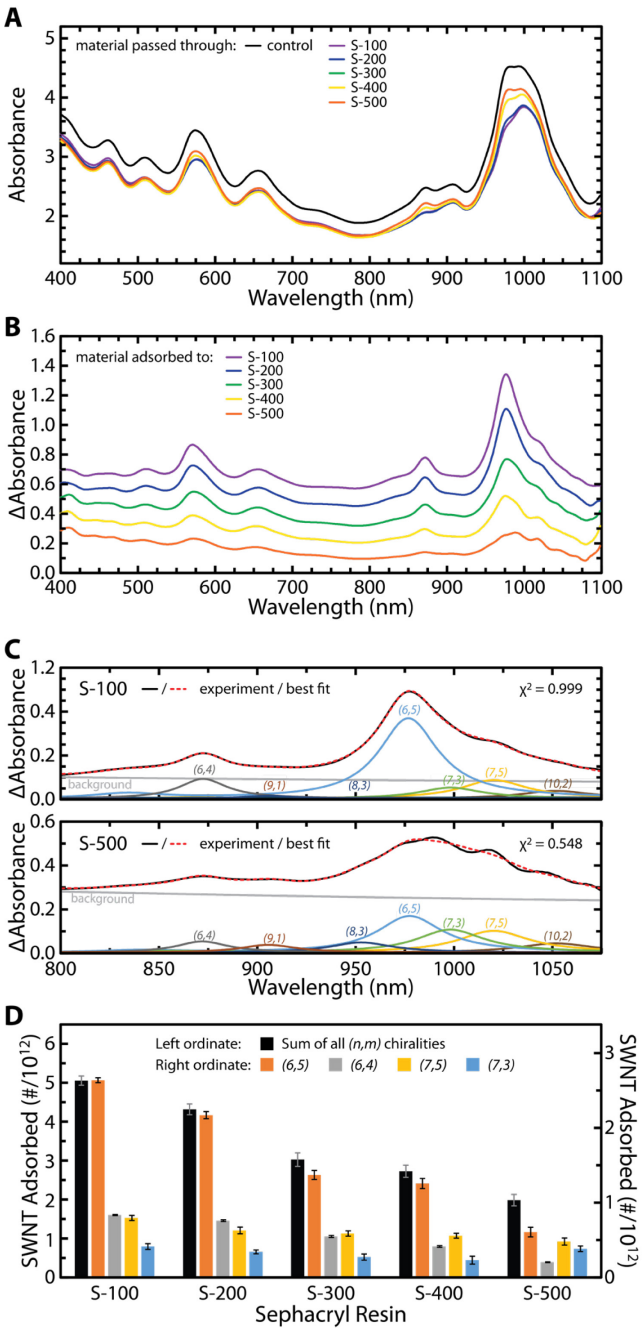

Fig. 4. Spectroscopic analysis of the SWNT materials adsorbed to each Sephacryl resin. (**A**) Absorbance spectra of SWNT suspensions after passing through Sephacryl columns of varying S-number alongside that after passing through a gel-free control. (**B**) Differential absorbance spectra with characteristic E_{11} absorbance peaks of adsorbed SWNT bound to each gel bed. (**C**) Per-chirality peak fitting of differential absorbance spectra affording per-chirality quantitation of adsorbed SWNT. (D) The total and per-chirality number of SWNT adsorbed to each resin. Triplicate spectra of data shown in panels (**A**) and (**B**) are provided in Supporting Information **Section S3** while the full height of error bars in (**D**) represent one standard deviation of triplicate measurement.

To independently assess SWNT material adsorbed to each Sephacryl formulation, differential absorbance spectroscopy was used whereby the spectrum of the SWNTs passing through a gel-containing column was subtracted from that of SWNTs passing through the gel-free (control) column, resulting in a calculated absorbance spectrum of SWNTs adsorbed to a given gel bed. The calculated spectra representing SWNTs adsorbed to each of five Sephacryl resins is shown in **Fig. 4B**, which demonstrates a clear trend of decreasing SWNT uptake by gels with larger Sephacryl S-number. The calculated spectra in **Fig. 4B** show distinct E_{11} absorbance peaks in the near infrared region, each of which corresponds to the absorbance of a given SWNT *(n,m)* chirality. Each spectrum was fit to a sum of Lorentzian line shapes of constant width and with SWNT *(n,m)* chirality dependent centers,[60] along with a linear background representative of amorphous carbon.[61] The resultant best fit, along with per-*(n,m)* chirality contribution to the collective spectrum, is shown for SWNT material adsorbed to Sephacryl S-100 (relatively high uptake) and Sephacryl S-500 (relatively low uptake) in **Fig. 4C**, while that of material adsorbed to the three other Sephacryl gels is shown in the **Supporting Information, Fig. S.3**. In each of these figures, the results of a Pearson χ^2 goodness-of-fit test is shown, where $0 \leq \chi^2 \leq 1$ and larger values of χ^2 represent increased likelihood that the data is distributed according to the model distribution.

The height of each deconvoluted chirality-specific peak can be combined with the experimentally determined per-chirality molar absorptivity and the assumption of a 300 nm length of each SWNT to calculate the absolute number of SWNTs adsorbed to each Sephacryl bed, both total and per *(n,m)* chirality. The numerical results of the best fit analyses of the calculated spectra shown in **Fig. 4B** in terms of per-chirality concentration for each fit performed, along with those of all best-fit analyses performed in this work (and the goodness of fit in the form of χ^2), are provided within a series of tables within **Supporting Information Section S4**. Importantly, SWNT synthesized *via* the CoMoCAT method,[62] containing primarily semiconducting species and enriched in the *(6,5)* chirality, were chosen for this study. This choice was made for two reasons: first, because hydrogel-based SWNT purification is well understood

to exclusively select for semiconducting SWNTs,[26,27] making use of SWNTs nearly free of metallic species both more efficient and still relevant to previous studies involving purification from other SWNT sources; and secondarily, use of *(6,5)* enriched CoMoCAT SWNTs ensures that only a handful of SWNT chiralities are present: *(6,5)*, *(6,4)*, *(7,5)*, *(7,3)*, *(10,2)*, *(8,3),* and *(9,1)*, the chirality dependent molar absorptivity of each of which has been reported.[63] Conversely, employment of either HiPCO[64] or non-*(6,5)* enriched CoMoCAT SWNTs would introduce semiconducting species with unknown values of molar absorptivity and hinder the accuracy of per-chirality quantitation of number of SWNTs. Nonetheless, a more thorough and robust study of the effects of different SWNT sources on hydrogel-based SWNT purification would be a worthwhile endeavor, but is reserved for another study.

The total (summed over all chiralities) number of SWNTs adsorbed to each gel is shown in the black bars (left ordinate) in **Fig. 4D**, which demonstrates the general trend of increased uptake of SWNT by Sephacryl gels with smaller S-numbers. This trend is relatively dramatic, with Sephacryl S-300 adsorbing approximately half of the SWNTs adsorbed by S-100, and S-500 adsorbing around half of that adsorbed by S-300. The per-chirality number of SWNTs adsorbed to each Sephacryl gel is shown in the colored bars (right ordinate) in **Fig. 4D** in terms of adsorption efficiency α, a unitless quantity ranging from 0-1 that relates the number of adsorbed SWNT to that of introduced SWNT:

$$\alpha = \frac{\#\ SWNT\ adsorbed\ to\ gel}{\#\ SWNT\ introduced\ to\ gel}. \qquad (3)$$

and emphasizes instances where large fractions of a given SWNT chirality are adsorbed due to high selectivity of that chirality by a given gel. The four chiralities with >10% abundance within the SWNT sample used in this study, *(6,5)*, *(7,3)*, *(6,4)*, and *(7,5)* are shown. Interestingly, the general trend of decreased uptake of SWNT by Sephacryl of larger S-number exists across all chiralities analyzed, demonstrating that the differences in SWNT uptake among the different Sephacryl formulations is not a chirality sensitive phenomenon.

In a recent report focused on studying mechanistic aspects of the chirality dependent interaction of SWNTs with Sephacryl S-200, we systematically varied the SDS concentration used during the adsorption event, showing a general decrease in SWNT uptake with higher SDS concentration that was largely independent of chirality.[45] This observation was attributed to the general increase of SDS order on the SWNT surface with increasing SDS concentration, which sterically hinders interaction between the SWNT sidewall and the gel surface.[65–67]

This phenomenon was explored in this study with each of the Sephacryl gels at both relatively high (105 mM) and low (26 mM) SDS concentrations during the adsorption event.

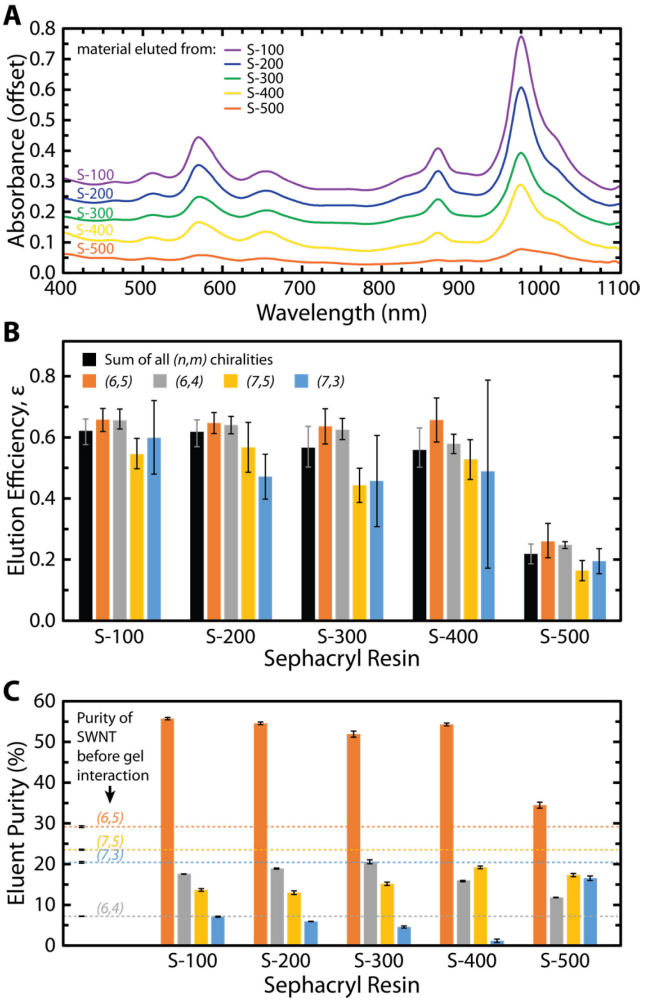

Fig. 5. Spectroscopic analysis of the SWNT materials eluted from each Sephacryl resin. (**A**) Absorbance spectra of SWNT suspensions eluted from each resin affords quantitation of per-chirality eluted SWNT *via* best-fit analysis of characteristic E_{11} absorbance peaks. (**B**) Elution efficiency summed over all SWNT chiralities along with that of the four most abundance chiralities adsorbed. (**C**) The per-chirality purity of the SWNT suspension introduced to each gel alongside that of SWNT eluted from each gel. Triplicate spectra of data shown in panel (**A**) are provided in **Supporting Information Section S3** while the full height of error bars in (**B**) and (**C**) represent one standard deviation of triplicate measurement.

Similarly to the data shown in **Fig. 4** and that previously reported for Sephacryl S-200,[45] each Sephacryl series gel shows a general decrease of SWNT uptake in the presence of SDS concentrations above 70 mM, and does so in a generally chirality independent manner, see Supporting Information **Section S5**.

Following adsorption and washing, a neat aqueous solution of relatively higher SDS concentration (170 mM) was added to the top of each gel bed to elute a fraction of adsorbed SWNT. The spectra of eluted materials from each gel is shown in **Fig. 5A**. The quantitative results of spectral deconvolution were considered in terms of elution efficiency ε,

$$\varepsilon = \frac{\#\ SWNT\ eluted\ from\ gel}{\#\ SWNT\ adsorbed\ to\ gel}, \quad (4)$$

which ranges from 0 to 1. The elution efficiency assesses both the overall efficiency gel-based SWNT purification, chiral specificity, and affords analysis into the chiral dependence of SWNT/gel interactions.

We have shown previously that while hydrogels composed of different polymeric backbones and bifunctional crosslinkers can afford chirally selective SWNT purification, chiral selectivity can occur during the adsorption event (Sephacryl resin), the elution event (Superose resin), or a combination of the two (Agarose media).[35] A collective comparison of adsorption efficiency α and elution efficiency ε affords insight into the mechanism of gel-based purification of SWNT and can inform strategies to improve such methods through perturbation of either adsorption or elution conditions.[45]

The elution efficiency of each Sephacryl gel formulation is shown both in terms of total SWNTs (summed over all chiralities, black bars) and in terms of the four most abundant chiralities present (colored bars) in **Fig. 5B**. Sephacryl S-100 through S-400 are relatively efficient gels, each of which elute 45-50% of adsorbed material. Sephacryl S-500 is a relatively inefficient gel, eluting approximately 30% of adsorbed material. In terms of chirality dependent interactions, the overall grouping is driven primarily by the *(6,5)* and *(6,4)* chiralities, each of which elute with 45-60% efficiency for Sephacryl S-100 through S-400 and only with 20-30% efficiency for Sephacryl S-500. In contrast, both the *(7,3)* and *(7,5)* chiralities elute with similar efficiency for every Sephacryl formulation, at about 25% and 45%, respectively.

The combination of initial abundance of each *(n,m)* chirality and per-chirality adsorption and elution efficiency collectively results in the per-chirality fractional purity within a given eluent:

$$f_{(n,m)} = \frac{\#\ SWNT\ (n,m)\ eluted\ from\ gel}{\sum_{(n,m)} \#\ SWNT\ (n,m)\ eluted\ from\ gel}. \quad (5)$$

The maximum elution $f_{(n,m)}$ is a quantitative measure of how chirally pure the eluent from a given SWNT/gel interaction is and remains the parameter-of-merit in terms of designing and optimizing gel-based SWNT purification methods. The per-chirality fractional purity of eluents obtained from each Sephacryl gel formulation is shown for the four most abundant chiralities present (colored bars) in **Fig. 5C**. For each of the five Sephacryl resins investigated, *(6,5)* is the most abundant chirality in all eluents, with *(6,4)* being second most abundant chirality in eluents obtained from all gels except Sephacryl S-500.

In contrast to the gel overloading conditions commonly employed to purify SWNT using Sephacryl S-200, this study also explored underloading conditions to better understand mechanistic aspects of the SWNT/gel interaction. In our previous work we demonstrated that even in underloaded conditions in which ample gel exists to support adsorption of all SWNT introduced, a fraction of semiconducting SWNTs pass through the gel unabsorbed and do not adsorb to a second column containing an overabundance of free gel binding sites.[45] This phenomenon was attributed to a SWNT-exclusive property that prevents SWNTs from adsorbing to Sephacryl S-200, which may include SWNT length, degree and nature of structural defects, or inhomogeneities in SWNT/surfactant interactions. Therefore, performing so-called underloaded experiments with each type of Sephacryl resin affords understanding of how gels of differing composition interact with SWNT of inherently different chirality and gel-interaction properties. In other words, while an overloaded experiment allows SWNT to self-select based on the chirality specific affinity for the gel

Resin	SWNT Uptake at Saturation
S-100	2.47 ± 0.24 x 10^{10} SWNT/cm^2
S-200	2.05 ± 0.31 x 10^{10} SWNT/cm^2
S-300	1.49 ± 0.35 x 10^{10} SWNT/cm^2
S-400	1.33 ± 0.26 x 10^{10} SWNT/cm^2
S-500	8.6 ± 2.3 x 10^{9} SWNT/cm^2

Table 2. Maximum number of SWNT adsorbed per square centimeter of gel surface area. Saturation levels determined from fitting of spectroscopic data collected under overloading conditions, **Fig. 4**, with reported error representing one standard deviation of triplicate measurement.

surface (affording purification), underloading conditions can hypothetically accommodate all SWNTs introduced, and therefore provide mechanistic insight into the ability of different gels to interact with differing SWNT properties (other than chirality).

Underloaded experiments were normalized according to gel-type by consideration of the unique adsorption efficiency, α, of each gel measured upon introduction of 2.6 x 10^{13} SWNT in overloading conditions, as shown in **Figs. 4A and 4B**. Specifically, such an analysis afforded approximation of the maximum number of SWNT that could be taken up per cm^2 of Sephacryl S-100, S-200, S-300, S-400, and S-500, which is listed in **Table 2**. This analysis afforded normalization of SWNT/gel interaction in underloading conditions according to SWNT loading ratio:

$$\rho = \frac{\sum_{(n,m)} \#_{introduced\ SWNT,(n,m)}}{\#_{gel}} \qquad (6)$$

where $\#_{introduced\ SWNT,(n,m)}$ is the number of SWNT of chirality (n,m) introduced to a given gel bed and $\#_{gel}$ is the number of gel binding sites available for SWNT adsorption, as determined by surface area of gel employed and per-gel saturation levels listed in **Table 2**.

By creation of relatively tall beds of each Sephacryl gel that presented approximately 2,250 cm^2 of gel surface area each, a stock solution of SWNT was diluted to create SWNT suspensions of consistent chirality distribution and per-gel constant loading ratio ($\rho = 0.15$);thus, every gel bed had ample material present to accommodate 6.7 times the number of SWNTs introduced. SWNTs introduced under these conditions that pass through the gel bed do so not because of a lack of available gel sites, but rather, due to some SWNT specific property. Therefore, differences in behavior noted among the five Sephacryl formulations tested under these conditions have the potential to provide valuable mechanistic insight into the relationship between gel formulation and the SWNT/SDS complex.

A plot of the scaled absorbance spectra of SWNT suspensions that passed through each gel bed in underloading conditions is shown in **Fig. 6A** (following page), demonstrating that for all resins investigated, some SWNTs appear functionally unable to adsorb to Sephacryl-type hydrogels. The spectral

characteristics of adsorbed material were calculated by differential absorbance spectroscopy and are shown for each resin in **Fig. 6B**. Photographs depicting SWNTs passing through both Sephacryl S-100 and S-500 during the adsorption step in underloaded conditions are shown in **Fig. 6C**, while those of the two gels during elution are shown in **Fig. 6D**. In each case, the presence of unabsorbed SWNTs (despite the underloading conditions) and irreversibly bound SWNT (despite the elution conditions) are visible.

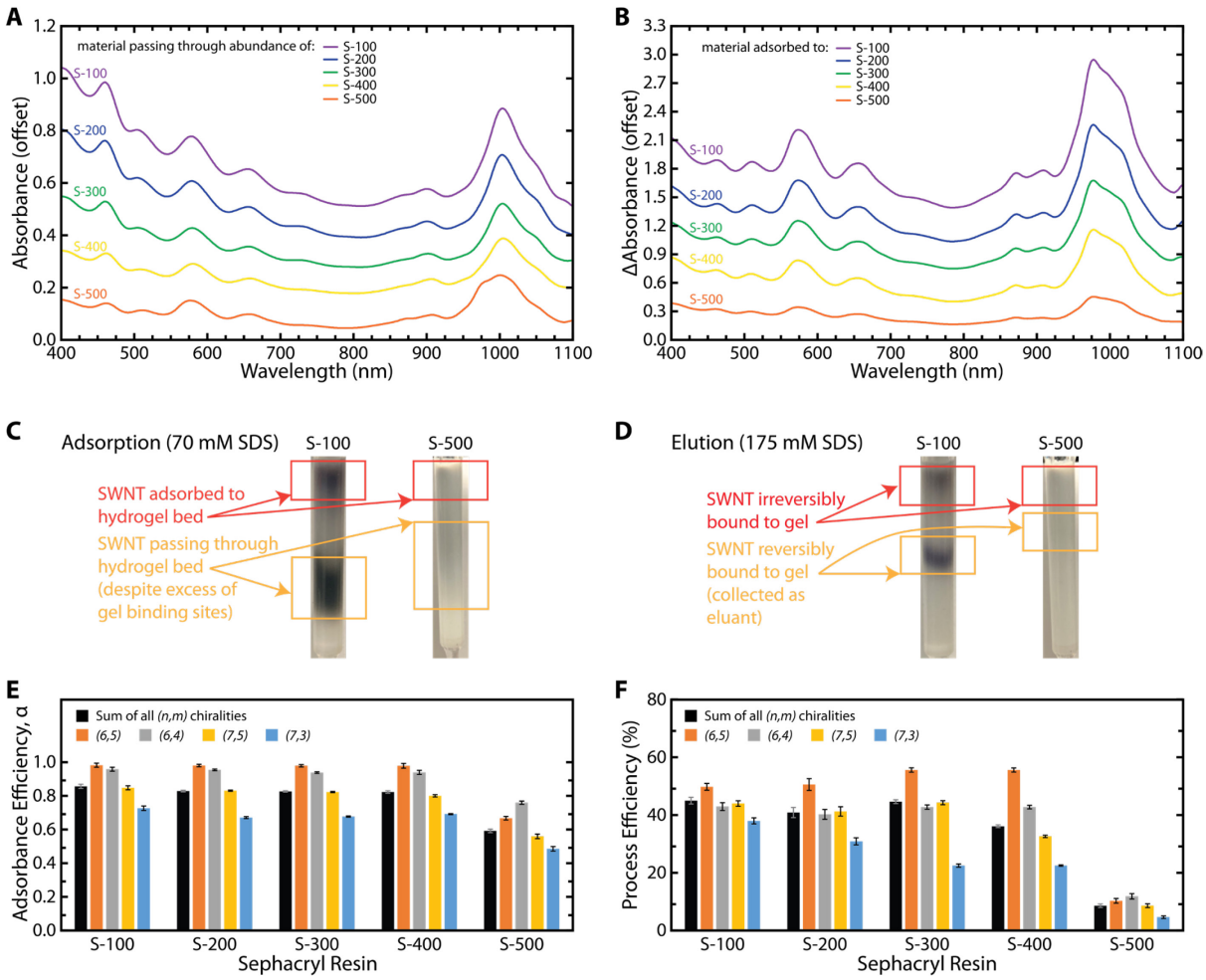

Fig. 6. Interaction of multi-chirality SWNT suspension with various Sephacryl resins in underloaded conditions. (**A**) Absorbance spectra of SWNT suspensions after passing through an overabundance of gel binding sites of each resin studied. (**B**) The calculated differential absorbance spectra of SWNT adsorbed to each Sephacryl resin under normalized underloading conditions. A representative experimental depiction of the adsorption (**C**) and elution (**D**) steps in an underloaded scheme for Sepacryl S-100 and S-500. The adsorption (**E**) and overall proccess (**F**) efficiency of each resin studied. Triplicate spectra of data shown in panels (**A**) and (**B**) are provided in **Supporting Information Section S3** while the full height of error bars in (**E**) and (**F**) represent one standard deviation of triplicate measurement.

Each of the spectra shown in **Figs. 6A and 6B**, along with corresponding spectra obtained by passing SWNTs through gel-free control columns, were deconvoluted by best-fit analysis to quantify both the total number of SWNTs introduced to and taken up by each gel type, which is shown graphically in terms of adsorption efficiency α in **Fig. 6E**. While there is no clear trend between Sephacryl of increasing S-number and overall SWNT adsorption efficiency, which falls within the range of 60-70% among these gels, there is a clear chiral *(n,m)* dependence on α between resins. Specifically, nearly 100% of the two most strongly adsorbing chiralities, *(6,5)* and *(6,4)*, was taken up by Sephacryl S-100 through S-400, while that amount diminished to ≈60% for S-500. Conversely, the adsorption efficiency of *(7,5)* and *(7,3)* remained in the 50-60% and 40-60% range, respectively, across all resins, showing no clear trend with Sephacryl S-number. Given the tendency of Sephacryl to exhibit chiral selectivity during the adsorption step[35] and its selection for the *(6,5)* and *(6,4)* chiralities amongst those present in this work, the S-100 through S-400 resins appear functionally unique from S-500.

The SWNTs eluted from each resin during underloaded conditions are shown graphically in terms of elution efficiency ε in **Fig. 6F**. A clear trend is present demonstrating that Sephacryl with smaller S-number elutes a greater fraction of adsorbed SWNT, with elution efficiency decreasing from 55 – 60% among Sephacryl S-100, S-200, and S-300, down to 36% for S-400 and 4% for S-500. There does not appear to be a strong deviation among per-chirality behavior in terms of elution efficiency among the resins studied, confirming for all Sephacryl resins that any chiral selectivity realized occurs during adsorption process as opposed to during elution.

Mechanistic Insights of this Study. Among the five Sephacryl resins studied, those with relatively smaller S-number have less surface roughness (smaller pores), a greater fraction of non-aqueous components present on the surface, and contain allyl dextran (aDEX) at a relatively larger density. Further, Sephacryl resins with relatively smaller S-number take up more SWNTs per gel surface area in overloading conditions, although with approximately the same chiral selectivity as do resins with larger S-number.

Approximately 50% of SWNTs adsorbed to resins S-100, S-200, S-300, and S-400 in overloading conditions eluted, while only 30% of those adsorbed to S-500 eluted. In normalized underloading conditions, a strong chiral selectivity is seen, with nearly 100% of the *(6,5)* and *(6,4)* chiralities adsorbed to S-100, S-200, S-300, and S-400 while only 65% of those introduced to S-500 are adsorbed.

Collectively, these results suggest that among Sephacryl resins, two independent parameters exist outside of SWNT chirality that significantly contribute to (and convolve) gel-based SWNT purification processes. The first parameter is surface density of aDEX, which correlates directly with the ability of a gel to adsorb SWNTs. Among gel components, aDEX has been speculated as responsible for SWNT binding sites at the gel surface.[36,37,39] This finding is further confirmed by our previous reports showing that increasing concentration of APS within otherwise equivalent Sephacryl-like gel formulations decreases SWNT uptake,[42] and the fact that hydrogel microparticles comprised exclusively of crosslinker MBA and APS adsorb little, if any, SWNT.[35] This finding is important, as the rational design of hydrogels for the improved purification of SWNT needs to consider mimicking or only slightly altering the chemical structure of this polysaccharide. Further, because aDEX constitutes the costliest component of Sephacryl, simply removing it from gel formulations to reduce costs will sacrifice SWNT/gel interaction.

The second parameter of outside of SWNT chirality that significantly affects gel-based purification is speculated here as SWNT-length, a property that has been discussed as potentially playing a role in SWNT-gel interaction in our earlier works. Specifically, nanotubes are expected to undergo cutting during prolonged tip-horn sonication,[68] which likely leads to a distribution of SWNT lengths among tubes of identical chirality (electronic structure). The correlation of SWNT length with *(n,m)* chirality has been speculated by others[69] and may find its origins in the chiral dependence of thermal stability,[70] which has been shown to correlate with smallest local curvature radius,[71] a property that strongly correlates with order of elution in gel-based purification schemes.[27]

This speculated role of SWNT length in SWNT-gel interaction is consistent with previous studies that have quantified both SWNT length and SWNT length distribution before and after interaction with Sephacryl gels of both relatively small (S-200[72–75] and large (S-500[76]) pore size. In each of these studies, SWNT of shorter lengths were either the first to adsorb to the gel or the last to pass through it (or be eluted from it), an observation indicative of a relatively stronger SWNT/gel interaction among relatively shorter SWNT. This is consistent with previous speculation that relatively long SWNT are, due to their length, unable to fully interact with the curved surface of a hydrogel microsphere, and thus bind less strongly.[33] While SWNT length is not probed directly in this work, it is nonetheless worthwhile to emphasize its speculated importance and the potential value of future work in which SWNT length is precisely measured, controlled, and correlated with critical parameters of gel-based SWNT purification.

In terms of the gels at the center of this investigation, it is expected that the fate of a SWNT/gel interaction is driven by the collective interaction between the SWNT sidewall and the hydrogel surface. Relatively short nanotubes would then be expected to bind to regions of the hydrogel surface with relatively high density of aDEX, which is more prevalent in Sephacryl gels of lower S-number (**Fig. 1**), causing those gels to adsorb more SWNT with an overall increase in reversible binding events (**Fig. 4**). In contrast, gels with rougher, more porous surfaces such as those of higher S-number (**Fig. 2**) have fewer regions of high aDEX density and can adsorb fewer SWNT per gel surface area (**Fig. 4**). In overloading conditions, the gel surface adsorbs only the SWNTs with the highest affinity for its aDEX-rich binding sites, demonstrating why similar SWNT populations (chirality distributions) adsorb and elute from Sephacryl S-100, S-200, S-300, and S-400 (**Fig. 5**). The exception is Sephacryl S-500, which has so little aDEX on its surface and such large pores, that a very small amount of only the most strongly adsorbing SWNTs become bound, leading to less efficient elution (**Fig. 5**). In underloading conditions, the speculated per-chirality distribution of SWNT length comes into play, with nearly 100% of SWNT of chiralities with small radius of bond curvature—*(6,4)* and *(6,5)*—binding to Sephacryl S-100, S-200, S-300, and S-400, potentially because

their shorter lengths allow for larger fractions of their tube length to interact with aDEX regions of the gel (**Fig 6**). However, with little aDEX on its surface and large pores, no chirality fully adsorbs to Sephacryl S-500, even in underloading conditions. Such underloading conditions ideally allow all thermodynamically driven binding events to occur, yet a smaller fraction of SWNTs elute from resins of increasing porosity. This is presumably because of the overabundance of binding sites available for SWNT binding, such that SWNTs that bind do so in aDEX rich sites, which are rare but nonetheless exist across all Sephacryl resins (**Fig 6**).

These concepts are summarized in **Fig. 7**, which illustrates the speculated interrelationship between surface density of aDEX and SWNT length. Specifically, longer SWNTs are not taken up by any of the Sephacryl resins regardless of aDEX surface density, while shorter SWNTs bind irreversibly to the gel surface regardless of aDEX surface density. In contrast, SWNTs of intermediate length interact with the Sephacryl resins differently depending on the availability of aDEX-rich binding sites. Importantly, not-illustrated in **Fig. 7** is SWNT chirality-dependent effects such as *(n,m)* specific electronic structure or *(n,m)* specific loading density and geometric arrangement of surfactant molecules, which are expected to be the primary drivers of SWNT/gel chirality-dependent interactions responsible for the achievement of scaled single-chirality purification using gel-based methods. A table comparing the convolved factors thought to play a significant role in SWNT-gel binding is shown in the **Supporting Information, Section S6**.

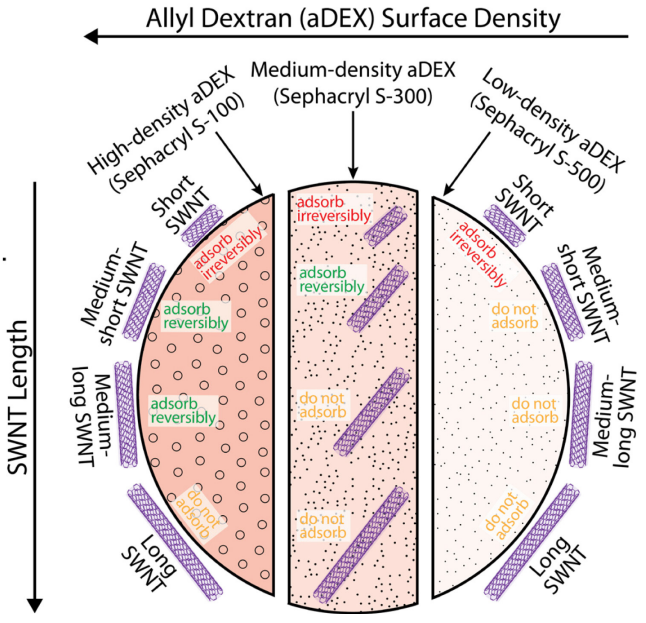

Fig. 7. Schematic diagram illustrating the two SWNT chirality-independent components speculated to play significant roles in gel-based SWNT purification: surface density of allyl dextran (aDEX) moieties and SWNT length.

Conclusions

Owing to the ability of Sephacryl S-200 to afford single-chirality purification of SWNTs, the ability of each of the five manufactured Sephacryl resins, which differ based on their manufacturer specified size exclusion properties, were investigated as SWNT purification media. This investigation focused on both the chemical and physical properties at the surface of each resin. Chemically, each resin was comprised of polysaccharide backbone aDEX, radical initiator APS, and crosslinker MBA, the latter two of which were determined to be present in approximately constant concentrations among the five formulations at approximately 80 mg/mL and approximately 10 mg/mL, respectively. The concentration of aDEX, however, decreases from approximately 80 mg/mL in S-100 down to 20 mg/mL in S-500. Physically, the pore size of each gel formulation was probed through quantification of swelling ratio and visualization of gel surface via SEM, which generally confirmed manufacturer specifications of larger pore sizes capable of fractionating larger biological macromolecules among gels of increasingly large Sephacryl S-number.

The ability of each resin to purify SWNTs through gel-based column chromatography schemes was determined by spectroscopic analysis of the SWNT solutions introduced to, passed through, and eluted from gel beds comprised of equal surface areas for each resin. Overloading conditions whereby introduced SWNTs compete for gel binding sites revealed that Sephacryl resins of lower S-number adsorb more SWNTs, with Sephacryl S-100 adsorbing (at an equivalent surface area) approximately 375% more SWNTs than Sephacryl S-500 and 130% more SWNTs than Sephacryl S-200, the standard material used in hydrogel-based SWNT purification. The chiral selectivity among SWNTs adsorbed to Sephacryl resins S-100 through S-400 was largely independent of Sephacryl formulation and demonstrated a general preference for adsorption of the *(6,4)* and *(6,5)* chiralities, while that of S-500 showed relatively less chiral selectivity. The chirality distribution of SWNTs eluted from each formulation largely mirrored that of the adsorbed material, however, Sephacryl S-500 eluted a smaller fraction of its adsorbed SWNTs (30%) compared with SWNT eluted from Sephacryl S-100 through S-400 (45-50%). Further, underloading

conditions whereby an approximately 6.7 times overabundance of gel binding sites exist relative to the number of introduced SWNTs revealed that the fraction of introduced SWNTs adsorbed was uniformly 60-70% for all gels, demonstrating the existence of a gel-independent (necessarily SWNTs or the SWNT/SDS complex) factor that inherently limits the adsorption of approximately one third of SWNTs.

Correlations between the physiochemical properties of each gel and its respective ability to purify SWNTs suggest that the surface porosity of a hydrogel largely dictates the efficiency with which it accommodates SWNTs, with gels of larger porosity able to accommodate less SWNTs due to a lack of aDEX (which affords binding) density on their surfaces.

These findings both expand the toolbox of gel-based SWNT purification, as they identify the superior performance of Sephacryl S-100 over the equivalently priced and near ubiquitously used Sephacryl S-200, in addition to serving as a roadmap for the development of hydrogel formulations tailored for SWNT purification. Specifically, future endeavors will focus on the synthesis, characterization, and SWNT-purification analysis of hydrogels comprised of aDEX, MBA, and APS that 1) are based on the Sephacryl-series formulations described here, and 2) deconvolute the gel-dependent chemical (aDEX *vs.* MBA) properties elucidated here from corresponding physical properties of the gel (porosity) through tailored control of each. Through improved understanding of chirality-dependent SWNT/gel interactions, gel formulations with superior SWNT-separation properties can be rationally designed and performance beyond that of Sephacryl realized, affording less expensive chirally pure SWNTs and/or SWNTs of higher chiral purity than that presently available.

Supporting Information

The Supporting Information is available free of charge at (insert link).

- Details of the atomistic model used to convert swelling ratio and elemental analysis data to concentrations of allyl dextran, methylene bis acrylamide, and ammonium persulfate in Sephacryl resins; manufacturer provided properties of Sephacryl resins and comparisons thereof; quantitative results from absorbance spectra deconvolutions generated and used in this work; and the effects of surfactant concentration on the purification characteristics of each Sephacryl resin in overloading conditions; and supporting references (insert PDF link)

Author Information

Corresponding Author

Kevin Tvrdy – Department of Chemistry & Biochemistry, University of Colorado at Colorado Springs, Colorado Springs, Colorado 80918, United States

ORCiID: Orcid.org/0000-0003-4949-3806

Email: ktvrdy@uccs.edu

Authors

Marshal Dolan – Department of Chemistry & Biochemistry, University of Colorado at Colorado Springs, Colorado Springs, Colorado 80918, United States

Laurique N Hughes – Department of Chemistry & Biochemistry, University of Colorado at Colorado Springs, Colorado Springs, Colorado 80918, United States

Acknowledgements

This material is based upon work supported by the National Science Foundation under grant no. 2107748. Additionally, MD acknowledges support from the UCCS Graduate School and KT thanks the UCCS BioFrontiers Center for instrumentation access.

References

(1) Saito, R.; Fujita, M.; Dresselhaus, G.; Dresselhaus, M. S. Electronic Structure of Chiral Graphene Tubules. *Appl. Phys. Lett.* **1992**, *60* (18), 2204–2206. https://doi.org/10.1063/1.107080.

(2) Kataura, H.; Kumazawa, Y.; Maniwa, Y.; Umezu, I.; Suzuki, S.; Ohtsuka, Y.; Achiba, Y. Optical Properties of Single-Wall Carbon Nanotubes. *Synth. Met.* **1999**, *103* (1–3), 2555–2558. https://doi.org/10.1016/S0379-6779(98)00278-1.

(3) Blancon, J.-C.; Paillet, M.; Tran, H. N.; Than, X. T.; Guebrou, S. A.; Ayari, A.; Miguel, A. S.; Phan, N.-M.; Zahab, A.-A.; Sauvajol, J.-L.; et. al. Direct Measurement of the Absolute Absorption Spectrum of Individual Semiconducting Single-Wall Carbon Nanotubes. *Nat. Commun.* **2013**, *4* (1), 2542. https://doi.org/10.1038/ncomms3542.

(4) O'Connell, M. J.; Bachilo, S. M.; Huffman, C. B.; Moore, V. C.; Strano, M. S.; Haroz, E. H.; Rialon, K. L.; Boul, P. J.; Noon, W. H.; Kittrell, C.; et. al. Band Gap Fluorescence from Individual Single-Walled Carbon Nanotubes. *Science* **2002**, *297* (5581), 593–596. https://doi.org/10.1126/science.1072631.

(5) Tang, D.-M.; Cretu, O.; Ishihara, S.; Zheng, Y.; Otsuka, K.; Xiang, R.; Maruyama, S.; Cheng, H.-M.; Liu, C.; Golberg, D. Chirality Engineering for Carbon Nanotube Electronics. *Nat. Rev. Electr. Eng.* **2024**, *1* (3), 149–162. https://doi.org/10.1038/s44287-023-00011-8.

(6) Schroeder, V.; Savagatrup, S.; He, M.; Lin, S.; Swager, T. M. Carbon Nanotube Chemical Sensors. *Chem. Rev.* **2019**, *119* (1), 599–663. https://doi.org/10.1021/acs.chemrev.8b00340.

(7) Yang, Z.; Xu, T.; Li, H.; She, M.; Chen, J.; Wang, Z.; Zhang, S.; Li, J. Zero-Dimensional Carbon Nanomaterials for Fluorescent Sensing and Imaging. *Chem. Rev.* **2023**, *123* (18), 11047–11136. https://doi.org/10.1021/acs.chemrev.3c00186.

(8) Hong, G.; Diao, S.; Antaris, A. L.; Dai, H. Carbon Nanomaterials for Biological Imaging and Nanomedicinal Therapy. *Chem. Rev.* **2015**, *115* (19), 10816–10906. https://doi.org/10.1021/acs.chemrev.5b00008.

(9) Yu, L.; Shearer, C.; Shapter, J. Recent Development of Carbon Nanotube Transparent Conductive Films. *Chem. Rev.* **2016**, *116* (22), 13413–13453. https://doi.org/10.1021/acs.chemrev.6b00179.

(10) Coleman, J. N.; Khan, U.; Blau, W. J.; Gun'ko, Y. K. Small but Strong: A Review of the Mechanical Properties of Carbon Nanotube–Polymer Composites. *Carbon* **2006**, *44* (9), 1624–1652. https://doi.org/10.1016/j.carbon.2006.02.038.

(11) Li, P.; Kumar, A.; Ma, J.; Kuang, Y.; Luo, L.; Sun, X. Density Gradient Ultracentrifugation for Colloidal Nanostructures Separation and Investigation. *Sci. Bull.* **2018**, *63* (10), 645–662. https://doi.org/10.1016/j.scib.2018.04.014.

(12) Feng, Y.; Miyata, Y.; Matsuishi, K.; Kataura, H. High-Efficiency Separation of Single-Wall Carbon Nanotubes by Self-Generated Density Gradient Ultracentrifugation. *J. Phys. Chem. C* **2011**, *115* (5), 1752–1756. https://doi.org/10.1021/jp1100329.

(13) Arnold, M. S.; Green, A. A.; Hulvat, J. F.; Stupp, S. I.; Hersam, M. C. Sorting Carbon Nanotubes by Electronic Structure Using Density Differentiation. *Nat. Nanotechnol.* **2006**, *1* (1), 60–65. https://doi.org/10.1038/nnano.2006.52.

(14) Arnold, M. S.; Stupp, S. I.; Hersam, M. C. Enrichment of Single-Walled Carbon Nanotubes by Diameter in Density Gradients. *Nano Lett.* **2005**, *5* (4), 713–718. https://doi.org/10.1021/nl050133o.

(15) Zheng, M.; Jagota, A.; Semke, E. D.; Diner, B. A.; Mclean, R. S.; Lustig, S. R.; Richardson, R. E.; Tassi, N. G. DNA-Assisted Dispersion and Separation of Carbon Nanotubes. *Nat. Mater.* **2003**, *2* (5), 338–342. https://doi.org/10.1038/nmat877.

(16) Huang, X.; Mclean, R. S.; Zheng, M. High-Resolution Length Sorting and Purification of DNA-Wrapped Carbon Nanotubes by Size-Exclusion Chromatography. *Anal. Chem.* **2005**, *77* (19), 6225–6228. https://doi.org/10.1021/ac0508954.

(17) Tu, X.; Zheng, M. A DNA-Based Approach to the Carbon Nanotube Sorting Problem. *Nano Res.* **2008**, *1* (3), 185–194. https://doi.org/10.1007/s12274-008-8022-7.

(18) Tu, X.; Manohar, S.; Jagota, A.; Zheng, M. DNA Sequence Motifs for Structure-Specific Recognition and Separation of Carbon Nanotubes. *Nature* **2009**, *460* (7252), 250–253. https://doi.org/10.1038/nature08116.

(19) Krupke, R.; Hennrich, F.; Weber, H. B.; Kappes, M. M.; V. Löhneysen, H. Simultaneous Deposition of Metallic Bundles of Single-Walled Carbon Nanotubes Using Ac-Dielectrophoresis. *Nano Lett.* **2003**, *3* (8), 1019–1023. https://doi.org/10.1021/nl0342343.

(20) Tanaka, T.; Jin, H.; Miyata, Y.; Kataura, H. High-Yield Separation of Metallic and Semiconducting Single-Wall Carbon Nanotubes by Agarose Gel Electrophoresis. *Appl. Phys. Express* **2008**, *1*, 114001. https://doi.org/10.1143/APEX.1.114001.

(21) Vetcher, A. A.; Srinivasan, S.; Vetcher, I. A.; Abramov, S. M.; Kozlov, M.; Baughman, R. H.; Levene, S. D. Fractionation of SWNT/Nucleic Acid Complexes by Agarose Gel Electrophoresis. *Nanotechnology* **2006**, *17* (16), 4263–4269. https://doi.org/10.1088/0957-4484/17/16/043.

(22) Xu, X.; Ray, R.; Gu, Y.; Ploehn, H. J.; Gearheart, L.; Raker, K.; Scrivens, W. A. Electrophoretic Analysis and Purification of Fluorescent Single-Walled Carbon Nanotube Fragments. *J. Am. Chem. Soc.* **2004**, *126* (40), 12736–12737. https://doi.org/10.1021/ja040082h.

(23) Fagan, J. A. Aqueous Two-Polymer Phase Extraction of Single-Wall Carbon Nanotubes Using Surfactants. *Nanoscale Adv.* **2019**, *1* (9), 3307–3324. https://doi.org/10.1039/C9NA00280D.

(24) Subbaiyan, N. K.; Cambré, S.; Parra-Vasquez, A. N. G.; Hároz, E. H.; Doorn, S. K.; Duque, J. G. Role of Surfactants and Salt in Aqueous Two-Phase Separation of Carbon Nanotubes toward Simple Chirality Isolation. *ACS Nano* **2014**, *8* (2), 1619–1628. https://doi.org/10.1021/nn405934y.

(25) Streit, J. K.; Lam, S.; Piao, Y.; Hight Walker, A. R.; Fagan, J. A.; Zheng, M. Separation of Double-Wall Carbon Nanotubes by Electronic Type and Diameter. *Nanoscale* **2017**, *9* (7), 2531–2540. https://doi.org/10.1039/C6NR09257H.

(26) Moshammer, K.; Hennrich, F.; Kappes, M. M. Selective Suspension in Aqueous Sodium Dodecyl Sulfate According to Electronic Structure Type Allows Simple Separation of Metallic from Semiconducting Single-Walled Carbon Nanotubes. *Nano Res.* **2009**, *2* (8), 599–606. https://doi.org/10.1007/s12274-009-9057-0.

(27) Liu, H.; Nishide, D.; Tanaka, T.; Kataura, H. Large-Scale Single-Chirality Separation of Single-Wall Carbon Nanotubes by Simple Gel Chromatography. *Nat. Commun.* **2011**, *2* (1), 309. https://doi.org/10.1038/ncomms1313.

(28) Wei, X.; Li, S.; Wang, W.; Zhang, X.; Zhou, W.; Xie, S.; Liu, H. Recent Advances in Structure Separation of Single-Wall Carbon Nanotubes and Their Application in Optics, Electronics, and Optoelectronics. *Adv. Sci.* **2022**, *9* (14), 2200054. https://doi.org/10.1002/advs.202200054.

(29) Tvrdy, K.; Jain, R. M.; Han, R.; Hilmer, A. J.; McNicholas, T. P.; Strano, M. S. A Kinetic Model for the Deterministic Prediction of Gel-Based Single-Chirality Single-Walled Carbon Nanotube Separation. *ACS Nano* **2013**, *7* (2), 1779–1789. https://doi.org/10.1021/nn305939k.

(30) Jain, R. M.; Tvrdy, K.; Han, R.; Ulissi, Z.; Strano, M. S. Quantitative Theory of Adsorptive Separation for the Electronic Sorting of Single-Walled Carbon Nanotubes. *ACS Nano* **2014**, *8* (4), 3367–3379. https://doi.org/10.1021/nn4058402.

(31) Liu, H.; Tanaka, T.; Urabe, Y.; Kataura, H. High-Efficiency Single-Chirality Separation of Carbon Nanotubes Using Temperature-Controlled Gel Chromatography. *Nano Lett.* **2013**, *13* (5), 1996–2003. https://doi.org/10.1021/nl400128m.

(32) Jain, R. M.; Ben-Naim, M.; Landry, M. P.; Strano, M. S. Competitive Binding in Mixed Surfactant Systems for Single-Walled Carbon Nanotube Separation. *J. Phys. Chem. C* **2015**, *119* (39), 22737–22745. https://doi.org/10.1021/acs.jpcc.5b07947.

(33) Watts, B. P.; Barbee, C. H.; Tvrdy, K. Exploiting the Physiochemical Interactions between Single-Walled Carbon Nanotubes and Hydrogel Microspheres To Afford Chirally Pure Nanotubes. *ACS Appl. Nano Mater.* **2019**, *2* (6), 3615–3625. https://doi.org/10.1021/acsanm.9b00567.

(34) Yang, D.; Li, L.; Li, X.; Xi, W.; Zhang, Y.; Liu, Y.; Wei, X.; Zhou, W.; Wei, F.; Xie, S.; et. al. Preparing High-Concentration Individualized Carbon Nanotubes for Industrial Separation of Multiple Single-Chirality Species. *Nat. Commun.* **2023**, *14* (1), 2491. https://doi.org/10.1038/s41467-023-38133-0.

(35) Zanoni, S.; Watts, B. P.; Tvrdy, K. Single-Walled Carbon Nanotube Chiral Selectivity Exhibited by Commercially Available Hydrogels of Varying Composition. *ACS Appl. Mater. Interfaces* **2021**, *13* (28), 33635–33643. https://doi.org/10.1021/acsami.1c06961.

(36) Clar, J. G.; Silvera Batista, C. A.; Youn, S.; Bonzongo, J.-C. J.; Ziegler, K. J. Interactive Forces between Sodium Dodecyl Sulfate-Suspended Single-Walled Carbon Nanotubes and Agarose Gels. *J. Am. Chem. Soc.* **2013**, *135* (47), 17758–17767. https://doi.org/10.1021/ja4052526.

(37) Clar, J. G.; Yuan, T.; Zhao, Y.; Bonzongo, J.-C. J.; Ziegler, K. J. Evaluation of Critical Parameters in the Separation of Single-Wall Carbon Nanotubes through Selective Adsorption onto Hydrogels. *J. Phys. Chem. C* **2014**, *118* (28), 15495–15505. https://doi.org/10.1021/jp503594h.

(38) Wang, G.; Wei, X.; Tanaka, T.; Kataura, H. Facile Synthesis of Guar Gum Gel for the Separation of Metallic and Semiconducting Single-Wall Carbon Nanotubes. *Carbon* **2018**, *129*, 745–749. https://doi.org/10.1016/j.carbon.2017.12.064.

(39) Wang, G.; Tanaka, T.; Wei, X.; Yudasaka, M.; Hirano, A.; Kataura, H. Directly Crosslinked Dextran Gels for SWCNT Separation. *Carbon* **2020**, *156*, 422–429. https://doi.org/10.1016/j.carbon.2019.09.081.

(40) Porath, J.; Flodin, P. Gel Filtration: A Method for Desalting and Group Separation. *Nature* **1959**, *183* (4676), 1657–1659. https://doi.org/10.1038/1831657a0.

(41) Toffaletti, J.; Savory, J.; Gitelman, H. J. Use of Gel Filtration to Examine the Distribution of Calcium among Serum Proteins. *Clin. Chem.* **1977**, *23* (12), 2306–2310. https://doi.org/10.1093/clinchem/23.12.2306.

(42) Dolan, M.; Watts, B. P.; Tvrdy, K. Tailored Synthesis of Hydrogel Media for Chirality Separation of Single Walled Carbon Nanotubes. *Carbon* **2021**, *171*, 597–609. https://doi.org/10.1016/j.carbon.2020.08.074.

(43) Holmberg, A.; Meurling, L. Preparation of Sulfhydrylborane-Dextran Conjugates for Boron Neutron Capture Therapy. *Bioconjug. Chem.* **1993**, *4* (6), 570–573. https://doi.org/10.1021/bc00024a023.

(44) Song, C.; Wang, P.; Makse, H. A. A Phase Diagram for Jammed Matter. *Nature* **2008**, *453* (7195), 629–632. https://doi.org/10.1038/nature06981.

(45) Watts, B. P.; Rolsma, C.; Dolan, M.; Tvrdy, K. Mechanism and Mitigation of Irreversible Material Loss within Gel-Based Single-Walled Carbon Nanotube Purification Schemes. *J. Phys. Chem. C* **2021**, *125* (47), 26084–26098. https://doi.org/10.1021/acs.jpcc.1c05832.

(46) Poenitzsch, V. Z.; Winters, D. C.; Xie, H.; Dieckmann, G. R.; Dalton, A. B.; Musselman, I. H. Effect of Electron-Donating and Electron-Withdrawing Groups on Peptide/Single-Walled Carbon Nanotube Interactions. *J. Am. Chem. Soc.* **2007**, *129* (47), 14724–14732. https://doi.org/10.1021/ja0750827.

(47) Shin, H.-J.; Kim, S. M.; Yoon, S.-M.; Benayad, A.; Kim, K. K.; Kim, S. J.; Park, H. K.; Choi, J.-Y.; Lee, Y. H. Tailoring Electronic Structures of Carbon Nanotubes by Solvent with Electron-Donating and -Withdrawing Groups. *J. Am. Chem. Soc.* **2008**, *130* (6), 2062–2066. https://doi.org/10.1021/ja710036e.

(48) White, B.; Banerjee, S.; O'Brien, S.; Turro, N. J.; Herman, I. P. Zeta-Potential Measurements of Surfactant-Wrapped Individual Single-Walled Carbon Nanotubes. *J. Phys. Chem. C* **2007**, *111* (37), 13684–13690. https://doi.org/10.1021/jp070853e.

(49) Nair, N.; Kim, W.-J.; Braatz, R. D.; Strano, M. S. Dynamics of Surfactant-Suspended Single-Walled Carbon Nanotubes in a Centrifugal Field. *Langmuir* **2008**, *24* (5), 1790–1795. https://doi.org/10.1021/la702516u.

(50) *Carbohydrate Analysis: High Performance Liquid Chromatography and Capillary Electrophoresis*; El Rassi, Z., Ed.; Journal of chromatography library; Elsevier: Amsterdam ; New York, 1995.

(51) David Pinz髇-Moreno, D.; Clidio Vicu駝-Galindo, E.; Gonz醴ez-Fern醬dez, J.; Soto-Gonzales, J.; Ver髇ica Carranza-Oropeza, M. Synthesis and Characterization of Hydrogels Based on Potato Starch/Poly(Vinyl Alcohol)/N,N'-Methylenebisacrylamide. *J. Renew. Mater.* **2022**, *10* (8), 2179–2201. https://doi.org/10.32604/jrm.2022.019793.

(52) Qayyum, Md.; Venkatram Reddy, B.; Ramana Rao, G. Vibrational Analysis of Mononitro Substituted Benzamides, Benzaldehydes and Toluenes. *Spectrochim. Acta. A. Mol. Biomol. Spectrosc.* **2004**, *60* (1–2), 279–290. https://doi.org/10.1016/S1386-1425(03)00227-0.

(53) Behari, K.; Agrawal, U.; Das, R. Gel Free Polymerization of N,N'-Methylenebisacrylamide Initiated by a Peroxodiphosphate-Thioacetamide Redox System. A Kinetic Study. *Polym. J.* **1993**, *25* (10), 1007–1013. https://doi.org/10.1295/polymj.25.1007.

(54) Da Silva, R. C.; De Aguiar, S. B.; Da Cunha, P. L. R.; De Paula, R. C. M.; Feitosa, J. P. A. Effect of Microwave on the Synthesis of Polyacrylamide-g-Chitosan Gel for Azo Dye Removal. *React. Funct. Polym.* **2020**, *148*, 104491. https://doi.org/10.1016/j.reactfunctpolym.2020.104491.

(55) Purama, R. K.; Goswami, P.; Khan, A. T.; Goyal, A. Structural Analysis and Properties of Dextran Produced by Leuconostoc Mesenteroides NRRL B-640. *Carbohydr. Polym.* **2009**, *76* (1), 30–35. https://doi.org/10.1016/j.carbpol.2008.09.018.

(56) Shingel, K. I. Determination of Structural Peculiarities of Dexran, Pullulan and γ-Irradiated Pullulan by Fourier-Transform IR Spectroscopy. *Carbohydr. Res.* **2002**, *337* (16), 1445–1451. https://doi.org/10.1016/S0008-6215(02)00209-4.

(57) Heyn, A. N. J. The Infrared Absorption Spectrum of Dextran and Its Bound Water. *Biopolymers* **1974**, *13* (3), 475–506. https://doi.org/10.1002/bip.1974.360130304.

(58) Park, H.; Guo, X.; Temenoff, J. S.; Tabata, Y.; Caplan, A. I.; Kasper, F. K.; Mikos, A. G. Effect of Swelling Ratio of Injectable Hydrogel Composites on Chondrogenic Differentiation of Encapsulated Rabbit Marrow Mesenchymal Stem Cells In Vitro. *Biomacromolecules* **2009**, *10* (3), 541–546. https://doi.org/10.1021/bm801197m.

(59) Antoniou, E.; Tsianou, M. Solution Properties of Dextran in Water and in Formamide. *J. Appl. Polym. Sci.* **2012**, *125* (3), 1681–1692. https://doi.org/10.1002/app.35475.

(60) Pfohl, M.; Tune, D. D.; Graf, A.; Zaumseil, J.; Krupke, R.; Flavel, B. S. Fitting Single-Walled Carbon Nanotube Optical Spectra. *ACS Omega* **2017**, *2* (3), 1163–1171. https://doi.org/10.1021/acsomega.6b00468.

(61) Naumov, A. V.; Ghosh, S.; Tsyboulski, D. A.; Bachilo, S. M.; Weisman, R. B. Analyzing Absorption Backgrounds in Single-Walled Carbon Nanotube Spectra. *ACS Nano* **2011**, *5* (3), 1639–1648. https://doi.org/10.1021/nn1035922.

(62) Monzon, A.; Lolli, G.; Cosma, S.; Mohamed, S. B.; Resasco, D. E. Kinetic Modeling of the SWNT Growth by CO Disproportionation on CoMo Catalysts. *J. Nanosci. Nanotechnol.* **2008**, *8* (11), 6141–6152. https://doi.org/10.1166/jnn.2008.SW21.

(63) Sanchez, S. R.; Bachilo, S. M.; Kadria-Vili, Y.; Lin, C.-W.; Weisman, R. B. (N,m)-Specific Absorption Cross Sections of Single-Walled Carbon Nanotubes Measured by Variance Spectroscopy. *Nano Lett.* **2016**, *16* (11), 6903–6909. https://doi.org/10.1021/acs.nanolett.6b02819.

(64) Bronikowski, M. J.; Willis, P. A.; Colbert, D. T.; Smith, K. A.; Smalley, R. E. Gas-Phase Production of Carbon Single-Walled Nanotubes from Carbon Monoxide via the HiPco Process: A Parametric Study. *J. Vac. Sci. Technol. Vac. Surf. Films* **2001**, *19* (4), 1800–1805. https://doi.org/10.1116/1.1380721.

(65) Ohfuchi, M. Ab Initio Study on Electronic Sorting of Single-Wall Carbon Nanotubes Using Sodium Dodecyl Sulfate. *J. Phys. Chem. C* **2018**, *122* (8), 4691–4697. https://doi.org/10.1021/acs.jpcc.7b12536.

(66) Blanch, A. J.; Quinton, J. S.; Shapter, J. G. The Role of Sodium Dodecyl Sulfate Concentration in the Separation of Carbon Nanotubes Using Gel Chromatography. *Carbon* **2013**, *60*, 471–480. https://doi.org/10.1016/j.carbon.2013.04.064.

(67) Silvera-Batista, C. A.; Scott, D. C.; McLeod, S. M.; Ziegler, K. J. A Mechanistic Study of the Selective Retention of SDS-Suspended Single-Wall Carbon Nanotubes on Agarose Gels. *J. Phys. Chem. C* **2011**, *115* (19), 9361–9369. https://doi.org/10.1021/jp111349x.

(68) Huang, Y. Y.; Terentjev, E. M. Dispersion of Carbon Nanotubes: Mixing, Sonication, Stabilization, and Composite Properties. *Polymers* **2012**, *4* (1), 275–295. https://doi.org/10.3390/polym4010275.

(69) Heller, D. A.; Mayrhofer, R. M.; Baik, S.; Grinkova, Y. V.; Usrey, M. L.; Strano, M. S. Concomitant Length and Diameter Separation of Single-Walled Carbon Nanotubes. *J. Am. Chem. Soc.* **2004**, *126* (44), 14567–14573. https://doi.org/10.1021/ja046450z.

(70) Miyata, Y.; Kawai, T.; Miyamoto, Y.; Yanagi, K.; Maniwa, Y.; Kataura, H. Chirality-Dependent Combustion of Single-Walled Carbon Nanotubes. *J. Phys. Chem. C* **2007**, *111* (27), 9671–9677. https://doi.org/10.1021/jp072359g.

(71) Li, J.; Jia, G.; Zhang, Y.; Chen, Y. Bond-Curvature Effect of Sidewall [2+1] Cycloadditions of Single-Walled Carbon Nanotubes: A New Criterion To the Adduct Structures. *Chem. Mater.* **2006**, *18* (15), 3579–3584. https://doi.org/10.1021/cm060563v.

(72) Miyata, Y.; Shiozawa, K.; Asada, Y.; Ohno, Y.; Kitaura, R.; Mizutani, T.; Shinohara, H. Length-Sorted Semiconducting Carbon Nanotubes for High-Mobility Thin Film Transistors. *Nano Res.* **2011**, *4* (10), 963–970. https://doi.org/10.1007/s12274-011-0152-7.

(73) Inori, R.; Okada, T.; Arie, T.; Akita, S. One-Pass Separation of Single-Wall Carbon Nanotubes by Gel Chromatography with a Gradient of Surfactant Concentration. *Nanotechnology* **2012**, *23* (23), 235708. https://doi.org/10.1088/0957-4484/23/23/235708.

(74) Thendie, B.; Miyata, Y.; Kitaura, R.; Miyauchi, Y.; Matsuda, K.; Shinohara, H. Rapid Single-Stage Separation of Micrometer-Long and High-Purity Semiconducting Carbon Nanotubes by Gel Filtration. *Appl. Phys. Express* **2013**, *6* (6), 065101. https://doi.org/10.7567/APEX.6.065101.

(75) Kim, D.; Ai Li, C.; Choi, K.-M. Interaction between Single-Walled Carbon Nanotubes and Chromatography Gel during Size Separation. *Mater. Res. Express* **2014**, *2* (1), 015004. https://doi.org/10.1088/2053-1591/2/1/015004.

(76) Arnold, K.; Hennrich, F.; Krupke, R.; Lebedkin, S.; Kappes, M. M. Length Separation Studies of Single Walled Carbon Nanotube Dispersions. *Phys. Status Solidi B* **2006**, *243* (13), 3073–3076. https://doi.org/10.1002/pssb.200669196.

TOC Graphic

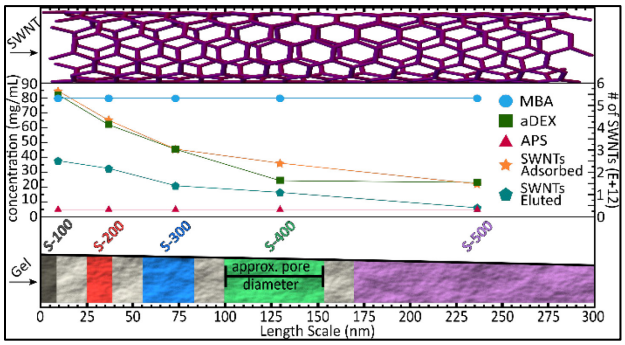
SWNT
concentration (mg/mL)
# of SWNTs (E+12)
MBA
aDEX
APS
SWNTs Adsorbed
SWNTs Eluted
S-100
S-200
S-300
S-400
S-500
Gel
approx. pore diameter
Length Scale (nm)